Journal of Molecular and Cellular Cardiology 111 (2017) 102–113

Contents lists available at ScienceDirect

Journal of Molecular and Cellular Cardiology

journal homepage: www.elsevier.com/locate/yjmcc

Spontaneous activation of a MAVS-dependent antiviral signaling pathway determines high basal interferon-β expression in cardiac myocytes

Efraín E. Rivera-Serrano[a,b,1], Nicole DeAngelis[a,b], Barbara Sherry[a,b,*]

[a] Department of Molecular Biomedical Sciences, College of Veterinary Medicine, North Carolina State University, Raleigh, NC, USA
[b] Comparative Medicine Institute, College of Veterinary Medicine, North Carolina State University, Raleigh, NC, USA

ARTICLE INFO

Keywords:
Cardiac myocyte
Cardiomyocyte
Interferon
Mitochondria
MAVS
MAM

ABSTRACT

Viral myocarditis is a leading cause of sudden death in young adults as the limited turnover of cardiac myocytes renders the heart particularly vulnerable to viral damage. Viruses induce an antiviral type I interferon (IFN-α/β) response in essentially all cell types, providing an immediate innate protection. Cardiac myocytes express high basal levels of IFN-β to help pre-arm them against viral infections, however the mechanism underlying this expression remains unclear. Using primary cultures of murine cardiac and skeletal muscle cells, we demonstrate here that the mitochondrial antiviral signaling (MAVS) pathway is spontaneously activated in unstimulated cardiac myocytes but not cardiac fibroblasts or skeletal muscle cells. Results suggest that MAVS association with the mitochondrial-associated ER membranes (MAM) is a determinant of high basal IFN-β expression, and demonstrate that MAVS is essential for spontaneous high basal expression of IFN-β in cardiac myocytes and the heart. Together, results provide the first mechanism for spontaneous high expression of the antiviral cytokine IFN-β in a poorly replenished and essential cell type.

1. Introduction

Viral myocarditis is recognized as the second leading cause of sudden death in young adults [25,29] and is found in approximately 10% of patients with unexplained heart failure [7]. Although most cases resolve spontaneously, viral myocarditis can progress to dilated cardiomyopathy and cardiac failure [16,29]; the latter representing one of the major causes of morbidity and mortality worldwide [11]. The unimpeded cardiac access afforded to viruses during viremia as well as the severely limited capacity of cardiac myocytes to enter the mitotic cycle [92] contribute to the particular vulnerability of the heart to viruses.

Type I interferon (IFN-α/β) treatment can be an effective therapeutic for human myocarditis [18,39,62,76], and defects in the host or cardiac myocyte IFN-α/β response aggravate virus-induced damage in mouse models of myocarditis and in primary cultures of cardiac myocytes [1,40,41,45,85]. While viral myocarditis can reflect immune-mediated damage to cardiac myocytes, most myocarditic viruses, including reovirus, induce direct cytopathic effects in these cells [7,29] and can induce myocarditis in the absence of the adaptive immune response [5,82–84]. For reovirus, the primary determinant of protection against virus-induced cardiac damage is the host IFN-α/β response [5,40,45,54,64,81,82,85,112]. Reovirus-induced cytopathic effect in primary cultures of murine cardiac myocytes accurately recapitulates both reovirus strain-specific differences in induction of myocarditis and the critical role for IFN-α/β [5,45,85]. We have previously shown that cardiac myocytes express higher basal levels of IFN-α/β than cardiac fibroblasts do, whereas the latter are more responsive to IFN-α/β signaling [54,87,111]. This integrated signaling network helps to pre-arm poorly replenishable cardiac myocytes and amplify antiviral signaling in cardiac fibroblasts to eliminate the viral infection [111]. However, the mechanism by which cardiac myocytes express high basal levels of IFN-β has not been elucidated.

Viral induction of IFN-α/β expression is initiated when a stimulus such as viral RNA is recognized by its sensors, in this case retinoic acid inducible gene-I (RIG-I)-like receptors (RLRs), including RIG-I itself and melanoma differentiation-associated gene 5 (MDA5) [48,49,105]. RLRs then translocate from the cytosol to intracellular membranes to interact with the mitochondrial antiviral signaling (MAVS; also known as IPS-1,

Abbreviations: ER, endoplasmic reticulum; IFN, interferon; IKK, IκB kinase; ISG, interferon-stimulated gene; MAM, mitochondrial-associated ER membranes; MAVS, mitochondrial antiviral signaling; MDA5, melanoma differentiation-associated gene 5; MFN2, mitofusin2; MOI, multiplicity of infection; PFU, plaque-forming unit; PLA, proximity ligation assay; RIG-I, retinoic acid inducible gene-I; RLR, RIG-I-like receptors; SR, sarcoplasmic reticulum; TBK1, TANK-binding kinase 1; TRAF3, tumor necrosis factor (TNF) receptor-associated factor 3; TNF, tumor necrosis factor

* Corresponding author.
E-mail address: barbara_sherry@ncsu.edu (B. Sherry).
[1] Current address: Department of Microbiology and Immunology, University of North Carolina – Chapel Hill.

http://dx.doi.org/10.1016/j.yjmcc.2017.08.008
Received 29 November 2016; Received in revised form 31 July 2017; Accepted 14 August 2017
Available online 16 August 2017
0022-2828/

Cardif, and VISA) adapter protein and promote MAVS oligomerization [42,44,78,101,102]. MAVS localizes primarily to the outer mitochondrial membrane [78], but also to peroxisomes [22] and to specialized domains of the endoplasmic reticulum (ER) that are in constant communication with the mitochondria [42]. These mitochondrial-associated ER membranes (MAM) are an important site for induction of IFN-α/β expression and inflammatory signaling [42,43,110]. When components of the MAVS pathway translocate to the MAM they induce IFN-α/β expression [42,43,55]. In contrast, peroxisomal MAVS plays a role in induction of IFN-λ expression in mucosal and epithelial cells [6,21,30,42,94]. Interactions of MAVS at the MAM activates the E3 ubiquitin ligase tumor necrosis factor (TNF) receptor-associated factor 3 (TRAF3) [38,65,91], which activates TANK-binding kinase 1 (TBK1) [32,37,79] and members of the IκB kinase (IKK) family [71,103,107]. These kinases then phosphorylate and activate the transcription factors IRF3, ATF-2/c-Jun and NF-κB; all of which are required for maximal IFN-α/β expression [57,97]. Secreted IFN-α/β then binds its receptor and induces expression of IFN-stimulated genes (ISGs), most of which have direct antiviral properties [20,75].

The identification of MAVS as a critical mitochondrial adapter for IFN-β expression introduced mitochondria as essential components in the IFN-β response [2,61,78,102]. While MAVS is ubiquitously expressed, its expression is much higher in cardiac and skeletal muscle compared to other organs and tissues [102], suggesting cells with abundant mitochondria might have an enhanced IFN-β response. Indeed, ectopic expression of MAVS in other cell types induces IFN-β expression through spontaneous activation of IRF3 and NF-κB [61,78,102]. We therefore hypothesized that differences in MAVS abundance and localization in cardiac myocytes might drive spontaneous downstream signaling and expression of IFN-β in the absence of viral infection.

Here, we used primary cultures of murine cardiac and skeletal muscle cells to identify differences between skeletal and cardiac muscle cells, and to identify the mechanism for high basal IFN-β expression in cardiac myocytes. First, we found that skeletal muscle cells do not express high basal levels of IFN-β, indicating that this is not characteristic of muscle cells in general. Remarkably, in unstimulated cardiac myocytes but not cardiac fibroblasts or skeletal muscle cells, MAVS is spontaneously activated to associate with the MAM resulting in activation of TRAF3 and TBK1. Accordingly, MAVS expression is required for high basal IFN-β expression in cardiac myocytes and in the adult heart. Together, results provide the first mechanism for spontaneous high expression of the antiviral cytokine IFN-β in a poorly replenished and essential cell type, and highlight a novel cell type-specific mitochondrial role in antiviral protection.

2. Materials and methods

2.1. Primary cardiac cell cultures

Timed-pregnant Cr:NIH(S) mice from the National Cancer Institute were maintained as a colony in a facility accredited by the Association for Assessment and Accreditation of Laboratory Animal Care. Wild-type C57BL/6, MAVS$^{-/-}$ [88], and RIG-I$^{-/-}$MDA5$^{-/-}$ [27] mice were maintained as an in-house colony and used for timed matings. The hearts of MAVS$^{-/-}$ mice were confirmed to be histologically and functionally normal (Fig. S1). All animal procedures were approved by the North Carolina State University Institutional Animal Care and Use Committee (IACUC). Primary cardiac cell cultures were generated as previously described [80] from 1-day-old neonatal and term fetal mice resulting from timed pregnancies. For RNA or protein harvest, cardiac myocyte and fibroblast cultures in Dulbecco MEM (DMEM; Gibco #11965-092) supplemented to contain 7% fetal calf serum (FCS; Atlanta Biologicals) and 10 μg/ml gentamycin (Sigma, #G1272) were plated at 1×10^6 or 5×10^5 cells per well in 24-well or 48-well clusters, respectively. For confocal microscopy, cardiac myocyte or cardiac fibroblast cultures were plated at 3.5×10^5 or 1.75×10^5 cells per chamber in 8-well poly-D-lysine-coated chamber slides (Corning), respectively. Cardiac myocyte cultures were also supplemented to contain 0.06% thymidine (to inhibit cardiac fibroblast growth). Cardiac myocyte and cardiac fibroblast cultures were ≥ 90% and ≥ 95% pure, respectively, as estimated by immunostaining against sarcomeric actin (alpha Sr-1) and vimentin, respectively (data not shown). In addition, RT-qPCR results (Fig. S2) confirmed that, as expected, cardiac fibroblast cultures expressed high levels of vimentin [9,53] and DDR2 [35,53,109] but expressed lower levels of α-myosin heavy chain than did cardiac myocyte cultures and lower levels of CD31 (a.k.a. PECAM-1) and VE-Cadherin (a.k.a. CDH5, CD144) than did vascular endothelial cells. For all experiments, cultures were incubated at 37 °C in 5% CO_2 for two days post-seeding before use, and were never passaged.

2.2. Primary skeletal muscle cultures

Timed-pregnant mice and mouse colonies for timed matings were maintained as above, and all procedures were IACUC-approved. Muscle from the limbs of neonatal mice < 24 h old was dissected away from other tissues into Hanks' balanced salt solution (HBSS; Corning, #21-023-CV), the HBSS was aspirated, and the muscle was minced with sterile scissors and incubated in freshly prepared 2% Type II collagenase (Worthington Biochemical, #LS004174) in HBSS for 30 min with vortexing every 10 min. Cells were pelleted by centrifugation at 1800 × *g* for 5 min at room temperature, resuspended in HBSS, and re-pelleted as above. Cells were resuspended in DMEM supplemented to contain 6% FCS, 2 mM L-glutamine (Corning #25-005-Cl), and 10 μg/ml gentamycin, and passed through a 100 μm cell strainer (Falcon, #352360). Cells resuspended to 4×10^5/ml in supplemented DMEM were plated at 8×10^5 cells per well in 24-well clusters for RNA or protein harvest, or 2.8×10^5 cells per chamber in 8-well poly-D-lysine-coated chamber slides for confocal microscopy. After incubation at 37 °C in 5% CO_2 for two days, media was replaced with DMEM supplemented as above (for undifferentiated skeletal muscle cell cultures) or DMEM supplemented as above but at 3% instead of 6% FCS (for differentiated skeletal muscle cell cultures). Cultures were incubated an additional two days before use to allow differentiation, and were never passaged.

2.3. Viral infections

CsCl-purified reovirus type 3 Dearing (T3D) was maintained as a low-passage laboratory stock and stored at − 80 °C. T3D was chosen as a strong inducer of IFN-α/β expression in cardiac cells [54,85,87] through the RIG-I/MAVS pathway [36,41]. For infections, cardiac cultures plated in 8-well chamber slides were inoculated with reovirus T3D at a multiplicity of infection (MOI) of 25 plaque forming units (PFU) per cell in 200 μl of supplemented DMEM. An additional 300 μl of supplemented DMEM was added after 1 h of incubation at 37 °C, and cells were fixed at 24 h post-infection. Mock-infected cultures were treated similarly but received supplemented DMEM as inocula.

2.4. Stimulation with Poly(I:C)

Cardiac fibroblasts were stimulated with 25 μg/ml Poly(I:C) (Invivogen; #tlrl-pic) using Lipofectamine 2000 (Thermo Fisher Scientific; #11668027) for a total of 4 h according to the manufacturer's instructions.

2.5. Antibodies

Antibodies used for immunoblotting and their corresponding dilutions were anti-MAVS (Santa Cruz Biotech sc-365334; 1:500), anti-TOM20 (Santa Cruz Biotech sc-11415; 1:300), anti-alpha Sr-1 (Abcam ab28052; 1:1500), anti-β-actin (Santa Cruz Biotech sc-1615-hrp,

1:2000), anti-MFN2 (Cell Signaling #9482; 1:800), anti-TBK1 (Cell Signaling #3504; 1:1000), anti-phospho-TBK1 (Ser172) (Cell Signaling #5483; 1:700), goat anti-rabbit IgG-HRP (Millipore #12-348; 1:2000), and goat anti-mouse IgG-HRP (Millipore #12-349; 1:2,000). Primary antibodies used for immunofluorescence were anti-MAVS (Santa Cruz Biotech sc-365,334; 1:100 dilution), anti-TOM20 (Abcam ab56783; 1:100 dilution), anti-FACL4 (Thermo PA5-27137; 1:50), anti-PMP70 (Abcam ab3424; 1:650), anti-MFN2 (Cell Signaling #9482; 1:50), anti-TRAF3 (Santa Cruz Biotech sc-1828or Thermo Fisher Scientific PA1-41107; 1:50), anti-alpha Sr-1 (Abcam ab28052; 1:50), anti-vimentin (Thermo Fisher Scientific PA1-16759; 1:2000), anti-GM130 (BD Biosciences #610822; 1:250), anti-reovirus σ1 5C6 and G5 ([95]; mix of 1:2500 each; Fig. 6B), and rabbit anti-reovirus T3D antisera (B. Sherry, unpublished; 1:2000; Fig. S5). Secondary antibodies were Alexa® 488-, Alexa® 594- or Alexa® 647-conjugated goat anti-mouse, anti-rabbit or anti-chicken IgG (Thermo Fisher Scientific; 1:750 - 1:1,000).

2.6. Indirect immunofluorescence

Cells in 8-well poly-D-Lysine-coated chamber slides were fixed in 4% paraformaldehyde (PFA; Electron Microscopy Sciences) in phosphate-buffered saline (PBS) for 20 min, and permeabilized with 0.25% Triton X-100 (Sigma, # × 100) in PBS at room temperature for 10 min. Slides were rinsed in PBS and blocked with 5% normal goat serum (Sigma; #G9023) diluted in PBS at room temperature for 60 min. Cells were then incubated in 300 nM DAPI (Sigma-Aldrich; #D8417) diluted in PBS for 20 min prior to immunostaining sequentially with the indicated primary antibodies diluted in 0.01% IgG- and protease-free BSA (Jackson ImmunoResearch Laboratories, Inc.) for 60 min each at room temperature. Slides were rinsed in PBS and incubated with the appropriate species-specific secondary antibodies for 60 min at room temperature. Slides were washed in PBS, and coverslips were mounted on slides using ProLong Gold (Invitrogen).

2.7. Reverse transcription - quantitative PCR (RT-qPCR)

Cells in 24-well clusters were lysed in RLT (Qiagen, Inc.). Alternatively, transverse mid-cardiac sections (27–41 mg) were disrupted in RLT using 1 mm zirconia/silica beads (Biospec, Inc.) in a mini-beadbeater (Biospec, Inc.) for 30 s, chilled on ice for 1 min, and then disrupted and chilled for 3 additional cycles. Beads were pelleted at 8000 × *g* for 3 min at 4 °C and cell lysate supernatants recovered. All cell lysates were further homogenized using a QIAshredder (Qiagen, Inc.) and total RNA was harvested using an RNeasy kit (Qiagen, Inc.). RNA was treated with RNase-free DNase I (Qiagen, Inc.) to remove genomic DNA prior to generation of cDNA by reverse transcription in a total reaction volume of 25 μl or 50 μl containing 5 μM oligo(dT); 1 × *Taq* buffer (Thermo Scientific); 7.5 mM $MgCl_2$; 1 mM dithiothreitol; 1 mM (each) deoxynucleotide triphosphate, 0.67 U/μl RNasin and 0.2 U/μl of avian myeloblastosis virus reverse transcriptase (Promega Corp.). For qPCR, 10 or 20% of the reverse transcription product was amplified on a LightCycler® 480 fluorescence thermocyler (Roche Life Science) in 96-well plates. Each 25 μl sample reaction in 96-well plates contained 1 × Quantitech SYBR green master mix (Qiagen, Inc.) and 0.3 μM (each) forward and reverse primers. Relative abundance of IFN-β was obtained by comparison to a standard curve generated from serial dilutions of a DNA standard and normalized to the expression of glyceraldehyde-3-phosphate dehydrogenase (GAPDH). Primer sequences for IFN-β and GAPDH transcripts and DNA standards have been previously published [87]. Primer sequences for vimentin, DDR2, α-myosin heavy chain, CD31 and VE-Cadherin are as indicated (Fig. S2).

2.8. SDS-PAGE and immunoblotting

Whole cell protein extracts were obtained by lysing cells plated in 24-well clusters using radioimmunoprecipitation assay (RIPA) lysis buffer (50 mM Tris HCl [pH 7.4], 1% NP-40, 0.25% sodium deoxycholate, 150 mM NaCl, 1 mM EDTA) supplemented to contain 1% sodium dodecylsulfate (SDS), a cocktail of protease and phosphatase inhibitors (Sigma-Aldrich; P8340 and P2850), and 1 mM phenylmethylsulfonyl fluoride (PMSF; Sigma-Aldrich, P7626). Cells were rocked on ice for 20 min and centrifuged at 14,000 × *g* at 4 °C for 10 min to remove cellular debris. A bicinchoninic acid (BCA) protein assay (Thermo Fisher Scientific) was used to calculate protein concentrations. A total of 10–20 μg of protein from each lysate was boiled for 5 min in 1 × Laemmli sample buffer and resolved using 7.5–15% SDS-polyacrylamide gel electrophoresis (SDS-PAGE). The resolved proteins were transferred to either nitrocellulose or polyvinylidene fluoride (PVDF) membranes in transfer buffer (48 mM Tris, 39 mM glycine, 0.04% SDS, and 20% methanol) for 20–45 min at 15 V in a semi-dry transfer apparatus (Bio-Rad). Membranes were then blocked for 1–3 h at room temperature with 5% milk or 5% bovine serum albumin (BSA; Sigma-Aldrich) in Tris-buffered saline (20 mM Tris HCl [pH 7.6], 137 mM NaCl) containing 0.05–0.2% Tween 20 (TBS-T) and probed with the indicated primary antibodies overnight at 4 °C. Membranes were washed 3–5 times with TBS-T buffer and incubated with the appropriate horse radish peroxidase- (HRP-) conjugated, species-specific secondary antibodies at room temperature for 1.5 h. Membranes were washed 3–5 times in TBS-T and proteins were visualized using Amersham enhanced chemiluminiscence (ECL) or ECL Plus kits according to the manufacturer's instructions. Membranes were exposed to film and scanned using an HP Scanjet G4050. Quantification of band intensity was determined using the LI-COR BioSciences Image Studio™ Lite Software (version 5.x); and the intensity value of each band of interest was normalized to the corresponding band intensity of β-actin.

2.9. MitoTracker® Red staining

Cells in 8-well poly-D-Lysine-coated chamber slides (BD Biosciences) were incubated in 200 nM MitoTracker® Red CMXRos (Thermo Fisher Scientific; #M7512) diluted in serum-free media for 30 min at 37 °C. Cells were then immediately fixed in 4% PFA and treated as for indirect immunofluorescence.

2.10. In situ Proximity Ligation Assay (PLA)

Cells in 8-well poly-D-Lysine-coated chamber slides were fixed in 4% PFA. Cells were then permeabilized in 0.25% Triton X-100 for 10 min at room temperature and blocked with Duolink® Blocking Solution for 1 h at room temperature. Slides were then incubated sequentially with primary antibodies against TRAF3 and MAVS or TOM20 diluted in 0.1% IgG- and protease-free BSA in PBS for 1 h at room temperature. For the PLA reactions, all incubations were performed in a 37 °C incubator with increased humidity according to the manufacturer's recommendations using the Duolink® *In Situ* Detection Regents Red kit (Sigma, DUO92101). Dried slides were mounted on Duolink® Mounting Medium with DAPI (DUO82040) and imaged by confocal microscopy as *Z*-stacks to image the total volume of each cell.

2.11. Confocal microscopy and image analysis

A Zeiss LSM 710 confocal microscope equipped with a 40 × C-apochromat/1.1 NA water immersion objective from the Cellular and Molecular Facility (CMIF) at NC State University was used for all experiments. The pinhole diameter was maintained at 1 Airy unit (A.U.) and all images were obtained using multitrack sequential scanning for each fluorophore to prevent bleed-through. The excitation/emission wavelengths during micrograph acquisition were 488 nm/492–554 nm for Alexa Fluor® 488, 561 nm/584–666 nm for Alexa Fluor® 594, MitoTracker® and PLA Duolink® Red, 633 nm/650–709 nm for Alexa

Fluor® 647, and 405 nm/407–507 nm for DAPI. Images were processed for presentation using Photoshop® CS4. Intensity plot profiles were generated using ImageJ software [74]. Quantification of cell area occupied by mitochondria and the scoring of PLA dots per cell were performed using the particle analysis tool of ImageJ. Pearson's co-localization indexes were obtained using ImageJ software and the Just Another Colocalisation Plugin (JACoP) module [8].

2.12. Statistical analysis

A Student's two-sample *t*-test (pooled variance) was applied using Systat software. Results were considered significant if the *P* value was < 0.05.

3. Results

3.1. Cardiac myocytes express high basal levels of IFN-β compared to cardiac fibroblasts and skeletal myotubes

Our laboratory previously reported that cardiac myocytes express higher basal levels of IFN-β, IFN-α4, and a subset of ISGs compared to cardiac fibroblasts [45,85,87,111]. Given the differences in cellular physiology between cardiac myocytes and cardiac fibroblasts, we first asked whether the high basal expression of IFN-β is specific to cardiac myocytes or a conserved antiviral response across muscle cell types. Primary cultures of murine cardiac myocytes, cardiac fibroblasts, and skeletal muscle (Fig. 1A) were analyzed for their expression of basal levels of IFN-β by RT-qPCR (Fig. 1B). Cardiac myocytes expressed two- to four-fold more IFN-β than cardiac fibroblasts did, and three- to nine-fold more IFN-β than differentiated skeletal muscle cells did. Results confirmed higher basal expression of IFN-β in cardiac myocytes than cardiac fibroblasts and demonstrated that this is not a conserved property of all muscle cells. Previous demonstration that cardiac myocytes express high basal IFN-β in cardiac sections from adult mice [111] and that an unusual association of NF-κB with the *cis*-Golgi in cultured neonatal cardiac myocytes is also detected in cardiac sections from adult mice [70] together provide evidence that neonatal cardiac myocyte cultures recapitulate events in this pathway that occur *in vivo* in adults.

3.2. Mitochondria and MAVS are more abundant in muscle cells than cardiac fibroblasts

Given that mitochondria are key organelles in innate immune signaling [2,99] and that cardiac myocytes display the highest mitochondrial density among cell types [34], we asked whether spontaneous signaling originating in this organelle was responsible for high expression of IFN-β in cardiac myocytes. Importantly, the mitochondrial-localized MAVS adaptor protein is highly expressed at the transcript level in muscle tissues [102]. Total levels of TOM20, a marker of outer mitochondrial proteins, and MAVS were evaluated by immunofluorescence (Fig. 2A–B) and immunoblot (Fig. 2C) in the different primary cultures. Both cardiac myocytes and skeletal muscle cells expressed higher levels of mitochondrial proteins, including MAVS, than did cardiac fibroblasts, indicating that mitochondrial and MAVS abundance alone is not sufficient to drive spontaneous expression of IFN-β. However, while the mitochondrial localization of MAVS was confirmed in our cardiac cultures, the morphology of the mitochondria in cardiac myocytes was strikingly different from that in the other cell types (Fig. 2D).

3.3. Mitochondria are highly associated with the MAM in cardiac myocytes

Skeletal muscle cells did not express high basal levels of IFN-β (Fig. 1B) but they did contain abundant mitochondria and express high levels of MAVS (Fig. 2A–C). Therefore, we next probed the association of mitochondria with other intracellular structures known to serve as platforms for MAVS-dependent innate immune signaling. Primary cultures were immunostained and analyzed for the association of mitochondria (TOM20) with the MAM (FACL4) and peroxisomes (PMP70). Mitochondria were intimately associated with the MAM specifically in cardiac myocytes (Fig. 3A–B), but not with peroxisomes (Fig. S3). Furthermore, the level of mitofusin2 (MFN2), a protein involved in mitochondrial fusion and ER-mitochondria tethering [19,46], was significantly higher in cardiac myocytes than the other cell types (Figs. 3C and S4), providing one potential mechanism for the increased contacts between these two organelles in cardiac myocytes. Notably, MAVS expression is not required for the association of mitochondria and the MAM nor the high levels of MFN2 in cardiac myocytes (Fig. S4). Together, results confirmed the intimate relationship between mitochondria and the MAM in cardiac myocytes, likely by the higher expression of tethering factors such as MFN2.

3.4. MAVS is highly associated with the MAM in cardiac myocytes

Given the intimate association of mitochondria with the MAM specifically in cardiac myocytes, we next probed MAVS localization. Primary cultures were immunostained and analyzed for the association of MAVS with the MAM and peroxisomes (Fig. 4A–B). Not surprisingly, the association of MAVS with either the MAM or peroxisomes in

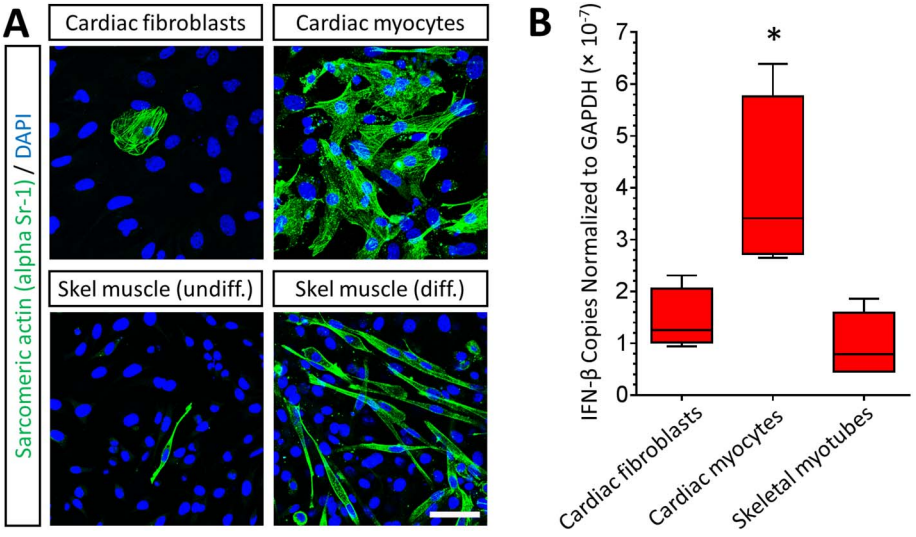

Fig. 1. Basal IFN-β expression is higher in cardiac myocytes than in cardiac fibroblasts and skeletal muscle cells. (A) Primary cultures of murine cardiac and undifferentiated (undiff.) and differentiated (diff.) skeletal muscle cells were generated from wild-type mice and were immunostained for the muscle-specific sarcomeric actin alpha Sr-1. Nuclei were counter-stained with DAPI. Scale bar = 50 μm. (B) RNA was harvested from the indicated cardiac cell or differentiated skeletal muscle cell primary cultures, analyzed by RT-qPCR, and copy number was normalized to GAPDH. Data are representative of means for two independent experiments from two independently generated primary cultures ± SD. *Significantly different from all others ($P < 0.05$).

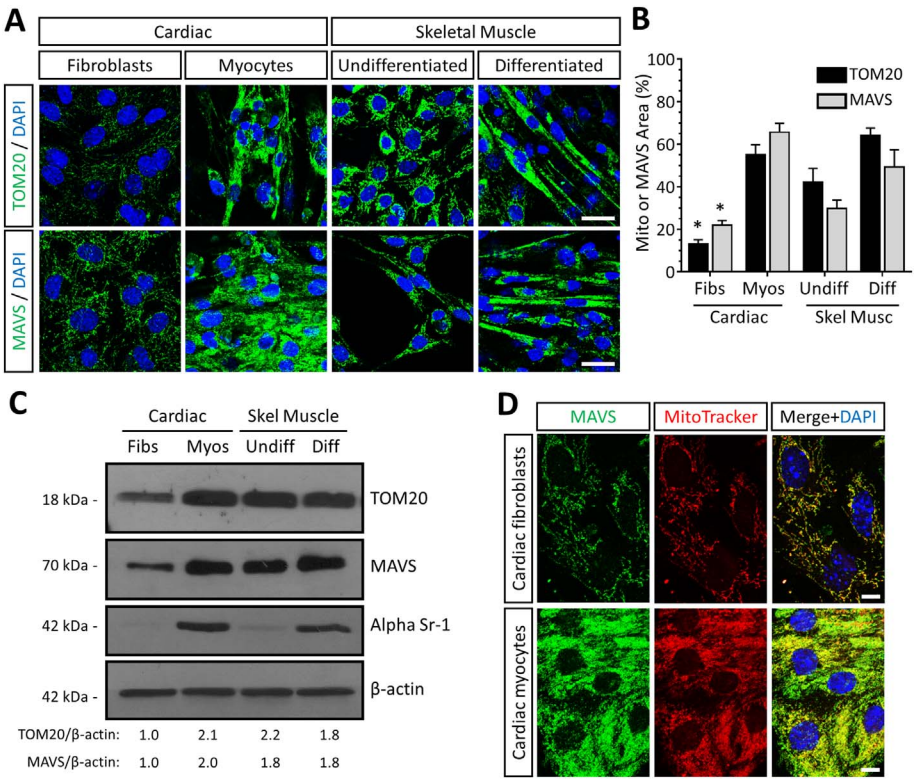

Fig. 2. Mitochondrial proteins and MAVS are more abundant in muscle cells than cardiac fibroblasts. (A) Primary cardiac or skeletal muscle cultures were immunostained with antibodies against TOM20 or MAVS. Nuclei were counterstained with DAPI. Scale bar = 50 μm. (B) Quantification of mitochondrial or MAVS density in the cell measured as the fraction of the cell occupied by either TOM20 or MAVS (mean ± SD; n = 6–12). *Significantly different from cardiac myocytes and skeletal muscle cells ($P < 0.05$). (C) Whole-cell protein extracts were harvested from the indicated primary cultures, resolved by SDS-PAGE, and immunoblotted using the indicated primary antibodies. Densitometry values for normalized TOM20 or MAVS band intensities are expressed relative to the band intensity of cardiac fibroblasts. (D) Primary cardiac cultures were incubated with MitoTracker®, fixed, and immunostained using an antibody against MAVS. Scale bar = 10 μm. Results are representative of at least two independent experiments.

unstimulated cardiac fibroblasts was minimal and reflected the mitochondrial localization of MAVS in these cells (Fig. 2A–B). To determine whether MAVS signaling occurs primarily through the MAM or peroxisomes in cardiac cells, cardiac fibroblasts were stimulated with Poly(I:C) by lipid-mediated transfection to activate RIG-I-dependent signaling. In stimulated cardiac fibroblasts there was significant association of MAVS with the MAM but not with peroxisomes (Fig. 4B), indicating that activation of RLRs in cardiac fibroblasts induces association of MAVS specifically with the MAM. Remarkably, MAVS co-localized with the MAM in unstimulated cardiac myocytes but not skeletal muscle cells to a degree similar to that in stimulated cardiac fibroblasts. Importantly, MAVS was not significantly associated with peroxisomes under any of the conditions tested (Fig. 4A–B) or upon RNA virus infection (Fig. S5B). Together, results indicate that the MAM, but not the peroxisome, is the primary site for MAVS-dependent signaling in cardiac cells and indicate that MAVS is highly associated with the MAM in cardiac myocytes.

3.5. MAVS is intimately associated with TRAF3 in unstimulated cardiac myocytes independent of RIG-I and MDA5 expression

Activated MAVS oligomerizes [44,101] and associates with members of the TRAF family, including the E3 ubiquitin ligase TRAF3 [42,56,69,89,93], and this interaction occurs as part of the MAVS signalosome at the MAM [42,55]. Thus, we asked whether MAVS localization to the MAM in cardiac myocytes results in its association with TRAF3. We used an *in situ* proximity ligation assay (PLA) which allows the visualization and quantitation of two individual proteins in close proximity in the form of fluorescent PLA dots [98]. Antibodies against TRAF3 and the mitochondrial protein TOM20 as a negative control did not generate significant PLA signals, confirming the specificity of the PLA and that abundant mitochondria in cardiac myocytes do not generate spurious PLA signals (Fig. 5). Antibodies against MAVS and TRAF3 demonstrated that these two proteins are found in close proximity in unstimulated cardiac myocytes but not in cardiac fibroblasts. Importantly, the primary cardiac cultures were derived from RIG-I$^{-/-}$MDA5$^{-/-}$ mice, indicating that expression of these upstream sensors is not required for the association of MAVS and TRAF3. Specificity was confirmed using cardiac cultures derived from MAVS$^{-/-}$ mice. In sum, results demonstrate that MAVS and TRAF3 are found in close proximity with each other in unstimulated cardiac myocytes and that this association is independent of RIG-I and MDA5.

3.6. TRAF3 is spontaneously activated in cardiac myocytes and its activation is MAVS-dependent

The observation that TRAF3 is in close proximity with MAVS in unstimulated cardiac myocytes (Fig. 5) prompted us to ask whether this results in spontaneous activation of TRAF3. Cellular sensing of viral nucleic acid leads to fragmentation of the *cis*-Golgi, and the redistribution of TRAF3 to ER/Golgi-associated compartments is required for its ability to interact with MAVS [93]. Intracellular distribution of TRAF3 was used as a marker of its activation status in our primary cultures (Fig. 6). In unstimulated cardiac fibroblasts, TRAF3 localized diffusely throughout the cytoplasm, but upon stimulation with Poly (I:C), TRAF3 localized to punctate bodies in perinuclear compartments reminiscent of rearrangements of the Golgi (Fig. 6A). Infection of cardiac fibroblasts with reovirus T3D, a strong inducer of the RIG-I/MAVS pathway [36,41,85,87], induced a similar redistribution of TRAF3, and this redistribution was dependent on MAVS as the punctate bodies were absent in cultures derived from MAVS$^{-/-}$ mice (Fig. 6B). Remarkably, TRAF3 localized to similar punctate bodies in perinuclear compartments in unstimulated cardiac myocytes, suggesting spontaneous activation of TRAF3 in these cells (Fig. 6A). This redistribution of TRAF3 was specific to cardiac myocytes and was not observed in skeletal muscle cells. Finally, the spontaneous activation of TRAF3 in cardiac myocytes was MAVS-dependent (Fig. 6C; absence of TRAF3 punctate bodies in null mice) but independent of the upstream sensors RIG-I and MDA5 (Fig. 6D; presence of TRAF3 punctate bodies in null mice), consistent with results for MAVS-TRAF3 association (Fig. 5). Together, results demonstrate that TRAF3 is spontaneously activated in unstimulated cardiac myocytes and this activation requires the expression

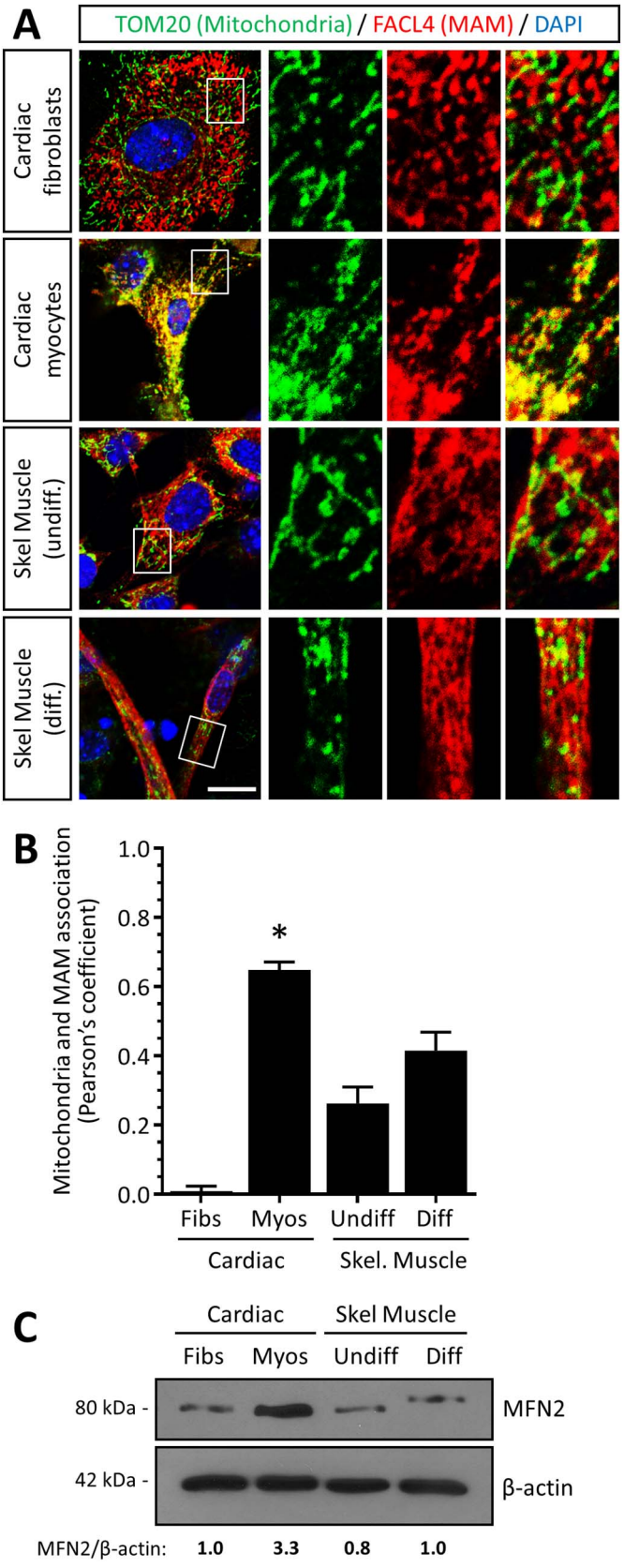

Fig. 3. Mitochondria are highly associated with the MAM in cardiac myocytes compared to cardiac fibroblasts and skeletal muscle cells. A) Primary cultures were immunostained with antibodies against TOM20 (mitochondria) and FACL4 (MAM); and nuclei were counterstained with DAPI. Images are representative of at least two independent experiments and > 10 cells analyzed per experiment. Scale bar = 10 μm. B) Pearson's co-localization coefficient (mean ± SEM; n = 8–12) of pixel overlap between TOM20 and FACL4. *, Significantly different from cardiac fibroblasts and skeletal muscle cells ($P < 0.05$). C) Whole-cell protein extracts from the indicated primary cultures were resolved by SDS-PAGE and immunoblotted using the indicated primary antibodies. Densitometry values for MFN2 band intensities normalized to actin are expressed relative to the band intensity of cardiac fibroblasts.

of MAVS but not the upstream viral RNA sensors RIG-I and MDA5.

3.7. TBK1 is spontaneously activated in cardiac myocytes and its activation is MAVS-dependent

MAVS-dependent stimulation of TRAF3 induces activation of TBK1, through phosphorylation of TBK1 at serine residue 172 [51] by either TBK1 itself or IKKβ [14]. To determine whether the spontaneous activation of MAVS-dependent signaling in cardiac myocytes (Figs. 5–6) resulted in activation of TBK1, the phosphorylation status of TBK1 was probed in our primary cultures (Fig. 7). TBK1 was phosphorylated specifically in cardiac myocytes but not in any of the other cell types analyzed, and phosphorylation was MAVS-dependent consistent with results for TRAF3 basal activation (Fig. 6C). Together, results indicate spontaneous activation of MAVS-dependent signaling in cardiac myocytes for phosphorylation of TBK1.

3.8. MAVS is a determinant of high basal expression of IFN-β in cardiac myocytes and the adult heart

Results indicated spontaneous activation of a MAVS-dependent signaling pathway in cardiac myocytes, suggesting that MAVS expression should be required for high basal expression of IFN-β in cardiac myocytes. Basal expression of IFN-β in cardiac cultures derived from either wild-type or MAVS$^{-/-}$ mice was measured by RT-qPCR (Fig. 8A). Results demonstrated a four-fold decrease in the basal levels of IFN-β in MAVS$^{-/-}$ cardiac myocytes compared to wild-type cells, but no difference in IFN-β expression between wild-type and MAVS$^{-/-}$ cardiac fibroblasts. Moreover, IFN-β expression was 18-fold lower in hearts from adult MAVS −/− mice than wild-type mice (Fig. 8B). Together, results demonstrate spontaneous activation of the MAVS signaling pathway in cardiac myocytes but not cardiac fibroblasts or skeletal muscle cells (Fig. 1) leading to spontaneous high basal expression of IFN-β (Fig. 8C).

4. Discussion

Cardiac myocytes constitute the majority of cell numbers and mass in the adult heart [4,90] yet in contrast to the vast majority of cell types, they rarely enter the cell cycle and display limited turnover throughout adulthood [86,108]. The heart lacks protective physical structures analogous to the blood-brain-barrier in the central nervous system, leaving cardiac cells vulnerable to numerous biotic and abiotic agents with the potential to compromise organ function. The innate IFN-β response represents a non-specialized yet critical antiviral response available to virtually every mammalian cell. Cardiac myocytes are exquisitely dependent on this innate response for their protection against viruses, and remarkably, have evolved a highly tuned regulation of this response for their protection. Specifically, cardiac myocytes express higher basal levels of IFN-β than do cardiac fibroblasts, and this basal IFN-β helps protect them against viral infection [45,85,87,111]. Here, we report the mechanism for high basal expression of IFN-β in cardiac myocytes: spontaneous activation of a MAVS-dependent signaling pathway likely originating at the MAM.

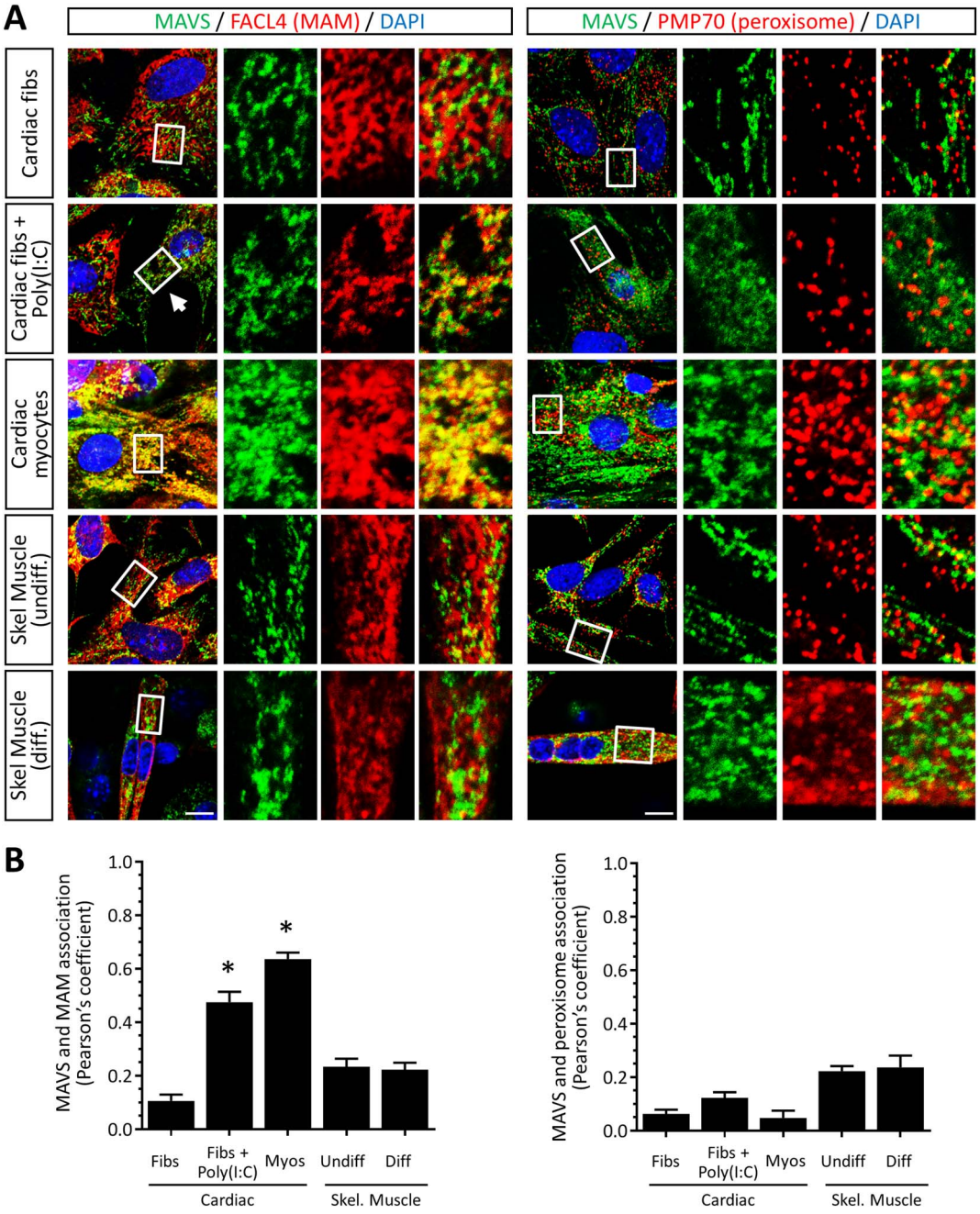

Fig. 4. MAVS is highly associated with the MAM, but not with peroxisomes, in stimulated cardiac fibroblasts and unstimulated cardiac myocytes. A) Primary cultures were immunostained with antibodies against MAVS and FACL4 (MAM) or PMP70 (peroxisome); and nuclei were counterstained with DAPI. Images are representative of at least two independent experiments and > 10 cells analyzed per experiment. Scale bar = 10 μm. B) Pearson's co-localization coefficient (mean ± SEM; n = 8–12) of pixel overlap between MAVS and FACL4 or PMP70. *Significantly different from cardiac fibroblasts and skeletal muscle cells ($P < 0.05$).

Cardiac myocytes express higher basal levels of IFN-β, IFN-α4, and a subset of ISGs than do cardiac fibroblasts [54,87,111]. Accordingly, cardiac myocytes express basal activation of the IFN-β signaling pathway as a pre-arming mechanism against viral infections [111]. The transcription factor IRF7 is an ISG that functions in a positive feedback loop to further induce IFN [72] and is expressed at higher basal levels in cardiac myocytes [87,111]. However, IRF7 function requires phosphorylation events that are triggered by viral infection [58,59,72] and, thus, IRF7 expression alone would likely be insufficient to induce strong expression of basal IFN in cardiac myocytes. Given that TBK1 is one kinase responsible for this phosphorylation [79], the MAVS-dependent spontaneous activation of TBK1 in cardiac myocytes (Fig. 7) could well be sufficient to activate IRF7 for amplification of basal IFN-β expression. Regulation of IRF7 function is complex [15,73], and the role of IRF7 in cardiac myocyte basal expression of IFN-β is ripe for study.

Cardiac myocytes have the highest density of mitochondria per cell volume, consistent with their high demand for energy [34]. Given that cardiac myocytes and skeletal myotubes have comparable levels of the mitochondria-associated protein MAVS (Fig. 2C) but express significantly different basal levels of IFN-β (Fig. 1B), MAVS abundance alone cannot be sufficient to drive spontaneous downstream signaling in cardiac myocytes. The mitochondria in cardiac myocytes are exceptionally well-associated with the sarcoplasmic reticulum (SR; the muscle-specific ER) to facilitate calcium (Ca^{2+}) transfer, reactive oxygen species (ROS) communication, and apoptotic signaling between

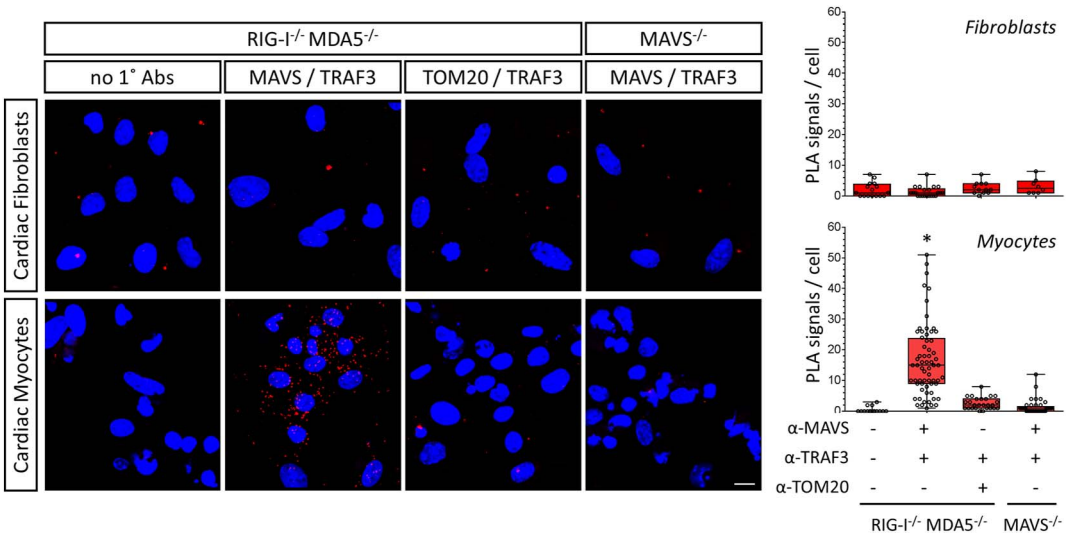

Fig. 5. MAVS and TRAF3 are intimately associated in unstimulated cardiac myocytes independently of RIG-I and MDA5 expression. Primary cardiac cultures generated from either RIG-I$^{-/-}$ MDA5$^{-/-}$ or MAVS$^{-/-}$ mice were fixed and subjected to an *in situ* proximity ligation assay (PLA) using the indicated primary antibodies and the respective species-specific secondary PLA probes. Confocal microscopy was used to obtain z-stack images of PLA signals (red) and nuclei (blue) representative of the total volume of the cells. Scale bar = 10 μm. The number of PLA signals per cell was quantified for each condition and each plotted value represents a single scored cell. *Significantly different from cardiac fibroblasts and skeletal muscle cells ($P < 0.05$).

these two organelles [10,23,26,33]. Our results suggest that the intrinsic association of the SR and mitochondria in cardiac myocytes likely facilitates the synthesis of basal IFN-β (Figs. 3–4). The association of these two organelles in cardiac myocytes may reflect the greater expression of the tethering factor MFN2 (Fig. 3C), although the role of MFN2 in ER-mitochondria interactions [19] has been recently debated [17,31,63]. Unfortunately, the essential roles of SR-mitochondrial contacts in regulating cardiac myocyte fate [67,68,96] prevent us from directly addressing their requirement for basal IFN-β expression. In addition, while siRNA-mediated or pharmacologic disruption of the MAM in other cell types enhances RIG-I signaling and IFN-β expression following viral infection, peroxisomal MAVS is concomitantly increased [42]. Thus, these methods would not be useful to provide additional evidence that the MAM is critical for high basal IFN-β expression in cardiac myocytes.

MFNs and mitochondrial fission and fusion can affect IFN expression, and viruses can modulate MFNs and mitochondrial dynamics. MFN1 is critical for mitochondrial fusion [24]. Viral activation of the MAVS signaling pathway is positively regulated by MFN1 [12,42,52,66] and induces mitochondrial elongation [12], and artificial enhancement of mitochondrial fusion can enhance IFN-β expression (12). While MFN2 can also induce mitochondrial fusion, it likely primarily functions as a tether between mitochondria and ER/SR membranes [24]. Interestingly, MFN2 represses viral induction of IFN-β expression [42,104], and does so independently of mitochondrial fusion or fission [42]. The high basal expression of IFN-β in cardiac myocytes which express high levels of MFN2 relative to cardiac fibroblasts (Figs. 3 and S4) suggests that MFN2 effects on IFN-β expression in cardiac cells differs from that in other cell types, consistent with evidence of many other cardiac-specific mitochondrial events [60]. Viruses can modulate MFNs and mitochondrial dynamics. For example, hepatitis B virus stimulates the degradation of MFN2 [50] and Dengue virus cleaves both MFN1 and MFN2 [106]. The effects of viruses on mitochondrial dynamics in cardiac cells has not been previously reported. Given that mitochondria in cardiac myocytes are basally associated with the MAM, we instead infected cardiac fibroblasts with reovirus T3D which induces high levels of IFN-β [45]. As expected, reovirus T3D induced MAVS association with the MAM (Fig. S5A) but not peroxisomes (Fig. S5B) in cardiac fibroblasts. Surprisingly however, reovirus T3D also induced mitochondrial shortening (Fig. S5C) suggesting either impairment of fusion or enhancement of fission. Indeed, the mitochondrial shortening was dramatic as evidenced by the markedly reduced size of most fluorescent "units" for both mitochondria and their associated MAVS. This mitochondrial shortening contrasts the correlation between mitochondrial elongation and IFN-β expression seen in several immortalized cell lines [12]. Results suggest that virus effects on mitochondrial dynamics differ between cardiac cells and other cell types, and warrant further investigation.

During viral infection, MAVS interacts with its downstream partner TRAF3 at the MAM [42]. Given that mitochondrial MAVS is highly associated with the MAM in unstimulated cardiac myocytes (Figs. 3–4), it is likely that the observed association between MAVS and TRAF3 (Fig. 5) occurs in these specialized cellular structures and serves as an initial trigger for TRAF3 activation. TRAF3 has been localized to compartments associated with the early secretory pathway, and stimulation of RIG-I results in fragmentation of the Golgi to punctate structures to facilitate TRAF3 interaction with MAVS [93]. These punctate structures are reminiscent of the ones present in unstimulated cardiac myocytes and in stimulated cardiac fibroblasts (Fig. 6). However, we were unable to detect co-localization of TRAF3 with the *cis*-Golgi marker GM130 (data not shown) as reported by others [93] and thus the origin and identity of these punctate bodies in cardiac cells remain unconfirmed. Importantly, the distribution of TRAF3 to these compartments in unstimulated cardiac myocytes is dependent on MAVS but not RIG-I and MDA5 (Fig. 6C–D), suggesting that signaling downstream of MAVS is required for fragmentation of specific domains of the Golgi. Notably, MAVS is required for *cis*-Golgi structure specifically in cardiac myocytes (Fig. S6) but not for the association of the mitochondria and the ER (Fig. S4). Whether the disruption of the *cis*-Golgi seen in MAVS$^{-/-}$ cardiac myocytes is direct or indirect (*e.g.* through regulation of Golgi structural proteins), and whether there are consequences to cardiac myocyte physiology has yet to be addressed.

To date, the only other cells that express high basal levels of type I IFN and ISGs are the neurons of the hippocampus [13,28], suggesting a role for basal IFN in the protection of susceptible non-dividing cells. High basal IFN in this cell type correlates with changes in abundance of components of the IFN signaling pathway during neuronal development and a concomitant increase in neuronal antiviral protection [28,77,100]. The specific type I IFN subtypes expressed at higher basal levels in these neurons are, however, different from the ones expressed

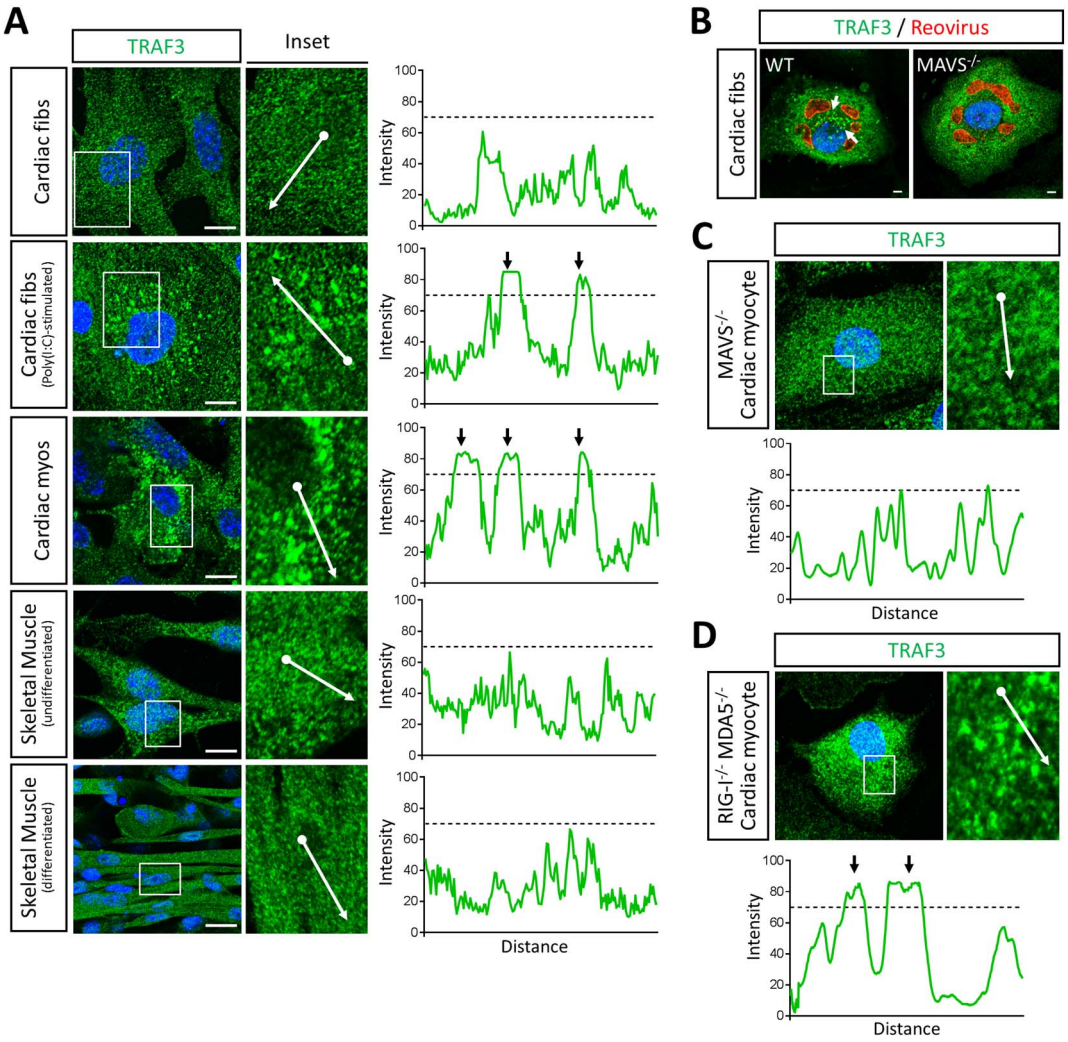

Fig. 6. TRAF3 is spontaneously activated in unstimulated cardiac myocytes and its activation is MAVS-dependent. A) Primary cultures were immunostained for TRAF3 and nuclei were counterstained with DAPI. Histograms display measured fluorescence intensity along the drawn line in the inset panels. B) Cardiac fibroblasts derived from either wild-type or MAVS$^{-/-}$ mice were infected with reovirus T3D and immunostained for TRAF3 and viral antigen. Arrows depict redistribution of activated TRAF3 to perinuclear punctate bodies upon virus infection. C,D) Cardiac myocytes generated from MAVS$^{-/-}$ (C) or RIG-I$^{-/-}$ MDA5$^{-/-}$ (D) mice were immunostained as in panel A. Scale bar = 10 μm. Results are representative of at least two independent experiments and > 20 cells per condition.

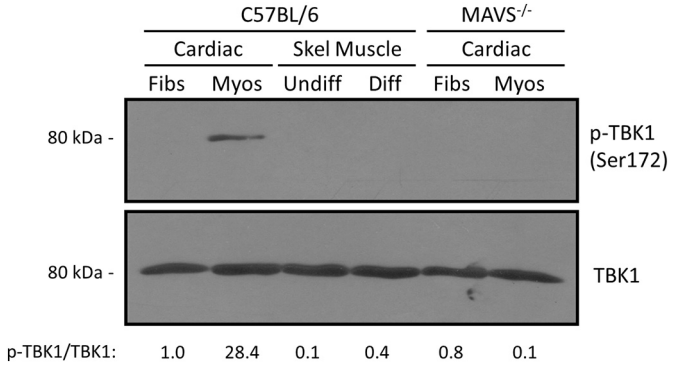

Fig. 7. TBK1 is activated in unstimulated cardiac myocytes and its activation is MAVS-dependent. Whole-cell protein lysates obtained from the indicated primary cultures were resolved by SDS-PAGE and immunoblotted with antibodies against TBK1 (total) or phosphorylated (p-)TBK1. Densitometry values for normalized p-TBK1 band intensities are expressed relative to the band intensity of wild-type cardiac fibroblasts.

in cardiac myocytes [13,54,87]. Despite these differences, cardiac myocytes and hippocampal neurons share striking similarities, including lower basal levels of latent STATs and reduced responsiveness to exogenous IFN-β compared to cardiac fibroblasts and mouse embryonic fibroblasts, respectively [13,111]. Thus, it appears that evolutionary forces have remodeled generalized antiviral signaling pathways for their specialization in highly susceptible and largely non-replenishable cell types.

Lastly, although the role of both mitochondria and the ER as platforms of antiviral responses in most cells has been extensively studied in many cell types [42,43,47,99], this report provides the first evidence that the enhanced SR-mitochondrial coupling that is characteristic of cardiac myocytes has an important role beyond muscle cell physiology. Specifically, results here highlight the critical role of SR-mitochondrial contacts for high basal IFN-β expression in the particularly vulnerable cardiac myocytes.

Funding

This research was supported by the National Institutes of Health grant AI083333 (B.S.), a Research Supplement to Promote Diversity in Health-Related Research through the parental R01 (B.S. and E.E.R-S.), and a U.S. Department of Education Graduate Assistance in Areas of National Need (GAANN) Fellowship (E.E.R-S.).

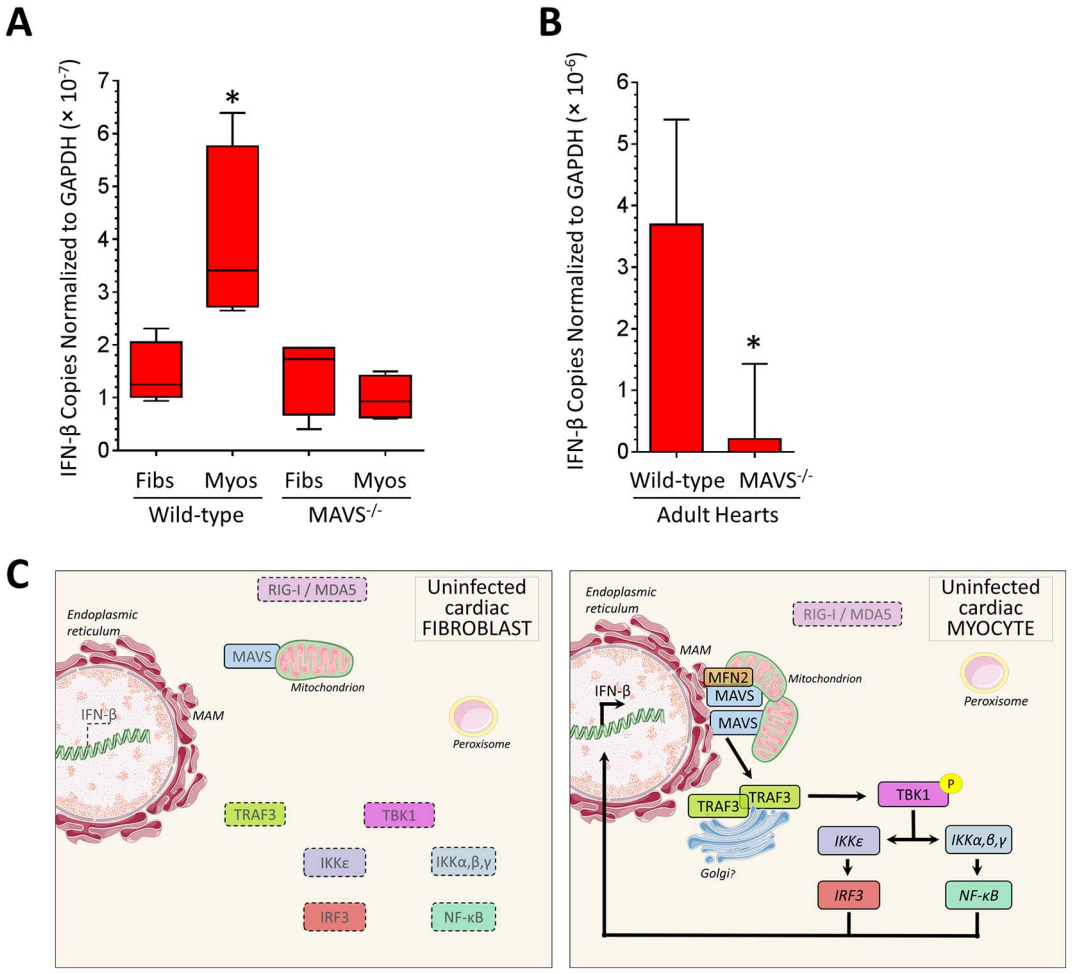

Fig. 8. MAVS is a determinant of high basal levels of IFN-β expression in cardiac myocytes and the adult heart. A) Primary cardiac myocytes and fibroblasts were generated from either wild-type or MAVS$^{-/-}$ mice. RNA was harvested and analyzed by RT-qPCR, and IFN-β copy number was normalized to GAPDH. Data are representative of means for two independent experiments from two independently generated primary cultures ± SD. *Significantly different from all others ($P < 0.05$). B) RNA was harvested from adult mouse hearts and analyzed by RT-qPCR. After background subtraction, IFN-β copy number was normalized to GAPDH. Data are means for 3–4 mice from two independent experiments ± SD. *Significantly different from wild-type ($P \leq 0.05$). C) Model for basal expression of IFN-β in cardiac cells. Inactive components are indicated by dashed borders and grey lettering. Components that were not directly assessed are indicated in italics.

Disclosures

None.

Acknowledgments

We thank Kimberly Parks and Rachael Van for helpful discussions; and Tiffany Benzine, Shannon Chiera, and Lance Johnson for excellent technical assistance. We thank Dr. Michael Gale Jr. (Univ. of Washington) for kindly providing the MAVS$^{-/-}$ and RIG-I$^{-/-}$ MDA5$^{-/-}$ mice; Dr. Ke Cheng for assistance with ultrasound, and Dr. John L. Parker (Cornell University) and members of Dr. Jennifer Luff's laboratory (NC State University) for insightful suggestions.

Appendix A. Supplementary data

Supplementary data to this article can be found online at http://dx.doi.org/10.1016/j.yjmcc.2017.08.008.

References

[1] N. Althof, S. Harkins, C.C. Kemball, C.T. Flynn, M. Alirezaei, J.L. Whitton, In vivo ablation of type I interferon receptor from cardiomyocytes delays coxsackieviral clearance and accelerates myocardial disease, J. Virol. 88 (2014) 5087–5099.
[2] D. Arnoult, F. Soares, I. Tattoli, S.E. Girardin, Mitochondria in innate immunity, EMBO Rep. 12 (2011) 901–910.
[4] I. Banerjee, J.W. Fuseler, R.L. Price, T.K. Borg, T.A. Baudino, Determination of cell types and numbers during cardiac development in the neonatal and adult rat and mouse, Am. J. Physiol. Heart Circ. Physiol. 293 (2007) H1883–1891.
[5] C.J. Baty, B. Sherry, Cytopathogenic effect in cardiac myocytes but not in cardiac fibroblasts is correlated with reovirus-induced acute myocarditis, J. Virol. 67 (1993) 6295–6298.
[6] S. Bender, A. Reuter, F. Eberle, E. Einhorn, M. Binder, R. Bartenschlager, Activation of type I and III interferon response by mitochondrial and peroxisomal MAVS and inhibition by hepatitis C virus, PLoS Pathog. 11 (2015) e1005264.
[7] L.A. Blauwet, L.T. Cooper, Myocarditis, Prog. Cardiovasc. Dis. 52 (2010) 274–288.
[8] S. Bolte, F.P. Cordelieres, A guided tour into subcellular colocalization analysis in light microscopy, J. Microsc. 224 (2006) 213–232.
[9] L.C. Boraas, T. Ahsan, Lack of vimentin impairs endothelial differentiation of embryonic stem cells, Sci Rep 6 (2016) 30814.
[10] R. Bravo-Sagua, A.E. Rodriguez, J. Kuzmicic, T. Gutierrez, C. Lopez-Crisosto, C. Quiroga, J. Diaz-Elizondo, M. Chiong, T.G. Gillette, B.A. Rothermel, S. Lavandero, Cell death and survival through the endoplasmic reticulum-mitochondrial axis, Curr. Mol. Med. 13 (2013) 317–329.
[11] A.L. Bui, T.B. Horwich, G.C. Fonarow, Epidemiology and risk profile of heart failure, Nat. Rev. Cardiol. 8 (2011) 30–41.
[12] C. Castanier, D. Garcin, A. Vazquez, D. Arnoult, Mitochondrial dynamics regulate the RIG-I-like receptor antiviral pathway, EMBO Rep. 11 (2010) 133–138.
[13] S.E. Cavanaugh, A.M. Holmgren, G.F. Rall, Homeostatic interferon expression in neurons is sufficient for early control of viral infection, J. Neuroimmunol. 279 (2015) 11–19.
[14] K. Clark, M. Peggie, L. Plater, R.J. Sorcek, E.R. Young, J.B. Madwed, J. Hough, E.G. McIver, P. Cohen, Novel cross-talk within the IKK family controls innate immunity, Biochem. J. 434 (2011) 93–104.
[15] R. Colina, M. Costa-Mattioli, R.J. Dowling, M. Jaramillo, L.H. Tai, C.J. Breitbach, Y. Martineau, O. Larsson, L. Rong, Y.V. Svitkin, A.P. Makrigiannis, J.C. Bell, N. Sonenberg, Translational control of the innate immune response through IRF-7,

Nature 452 (2008) 323–328.
[16] L.T. Cooper Jr., Myocarditis, N. Engl. J. Med. 360 (2009) 1526–1538.
[17] P. Cosson, A. Marchetti, M. Ravazzola, L. Orci, Mitofusin-2 independent juxtaposition of endoplasmic reticulum and mitochondria: an ultrastructural study, PLoS One 7 (2012) e46293.
[18] L. Daliento, F. Calabrese, F. Tona, A.L. Caforio, G. Tarsia, A. Angelini, G. Thiene, Successful treatment of enterovirus-induced myocarditis with interferon-alpha, J Heart Lung Transplant 22 (2003) 214–217.
[19] O.M. de Brito, L. Scorrano, Mitofusin 2 tethers endoplasmic reticulum to mitochondria, Nature 456 (2008) 605–610.
[20] M.J. de Veer, M. Holko, M. Frevel, E. Walker, S. Der, J.M. Paranjape, R.H. Silverman, B.R. Williams, Functional classification of interferon-stimulated genes identified using microarrays, J. Leukoc. Biol. 69 (2001) 912–920.
[21] S. Ding, M.D. Robek, Peroxisomal MAVS activates IRF1-mediated IFN-lambda production, Nat. Immunol. 15 (2014) 700–701.
[22] E. Dixit, S. Boulant, Y. Zhang, A.S. Lee, C. Odendall, B. Shum, N. Hacohen, Z.J. Chen, S.P. Whelan, M. Fransen, M.L. Nibert, G. Superti-Furga, J.C. Kagan, Peroxisomes are signaling platforms for antiviral innate immunity, Cell 141 (2010) 668–681.
[23] G.W. Dorn 2nd, L. Scorrano, Two close, too close: sarcoplasmic reticulum-mitochondrial crosstalk and cardiomyocyte fate, Circ. Res. 107 (2010) 689–699.
[24] G.W. Dorn 2nd, M. Song, K. Walsh, Functional implications of mitofusin 2-mediated mitochondrial-SR tethering, J. Mol. Cell. Cardiol. 78 (2015) 123–128.
[25] Y. Drory, Y. Turetz, Y. Hiss, B. Lev, E.Z. Fisman, A. Pines, M.R. Kramer, Sudden unexpected death in persons less than 40 years of age, Am. J. Cardiol. 68 (1991) 1388–1392.
[26] V. Eisner, G. Csordas, G. Hajnoczky, Interactions between sarco-endoplasmic reticulum and mitochondria in cardiac and skeletal muscle - pivotal roles in Ca(2)(+) and reactive oxygen species signaling, J. Cell Sci. 126 (2013) 2965–2978.
[27] J.S. Errett, M.S. Suthar, A. McMillan, M.S. Diamond, M. Gale Jr., The essential, nonredundant roles of RIG-I and MDA5 in detecting and controlling West Nile virus infection, J. Virol. 87 (2013) 11416–11425.
[28] J.R. Farmer, K.M. Altschaefl, K.S. O'Shea, D.J. Miller, Activation of the type I interferon pathway is enhanced in response to human neuronal differentiation, PLoS One 8 (2013) e58813.
[29] A.M. Feldman, D. McNamara, Myocarditis, N. Engl. J. Med. 343 (2000) 1388–1398.
[30] A.R. Ferreira, A.C. Magalhaes, F. Camoes, A. Gouveia, M. Vieira, J.C. Kagan, D. Ribeiro, Hepatitis C virus NS3-4A inhibits the peroxisomal MAVS-dependent antiviral signalling response, J. Cell. Mol. Med. 20 (2016) 750–757.
[31] R. Filadi, E. Greotti, G. Turacchio, A. Luini, T. Pozzan, P. Pizzo, Mitofusin 2 ablation increases endoplasmic reticulum–mitochondria coupling, Proc. Natl. Acad. Sci. 112 (2015) E2174–E2181.
[32] K.A. Fitzgerald, S.M. McWhirter, K.L. Faia, D.C. Rowe, E. Latz, D.T. Golenbock, A.J. Coyle, S.M. Liao, T. Maniatis, IKKepsilon and TBK1 are essential components of the IRF3 signaling pathway, Nat. Immunol. 4 (2003) 491–496.
[33] C. Garcia-Perez, G. Hajnoczky, G. Csordas, Physical coupling supports the local Ca2 + transfer between sarcoplasmic reticulum subdomains and the mitochondria in heart muscle, J. Biol. Chem. 283 (2008) 32771–32780.
[34] S. Goffart, J.C. von Kleist-Retzow, R.J. Wiesner, Regulation of mitochondrial proliferation in the heart: power-plant failure contributes to cardiac failure in hypertrophy, Cardiovasc. Res. 64 (2004) 198–207.
[35] E.C. Goldsmith, A. Hoffman, M.O. Morales, J.D. Potts, R.L. Price, A. McFadden, M. Rice, T.K. Borg, Organization of fibroblasts in the heart, Dev. Dyn. 230 (2004) 787–794.
[36] D. Goubau, M. Schlee, S. Deddouche, A.J. Pruijssers, T. Zillinger, M. Goldeck, C. Schuberth, A.G. Van der Veen, T. Fujimura, J. Rehwinkel, J.A. Iskarpatyoti, W. Barchet, J. Ludwig, T.S. Dermody, G. Hartmann, C. Reis e Sousa, Antiviral immunity via RIG-I-mediated recognition of RNA bearing 5′-diphosphates, Nature 514 (2014) 372–375.
[37] B. Guo, G. Cheng, Modulation of the interferon antiviral response by the TBK1/IKKi adaptor protein TANK, J. Biol. Chem. 282 (2007) 11817–11826.
[38] H. Hacker, V. Redecke, B. Blagoev, I. Kratchmarova, L.C. Hsu, G.G. Wang, M.P. Kamps, E. Raz, H. Wagner, G. Hacker, M. Mann, M. Karin, Specificity in Toll-like receptor signalling through distinct effector functions of TRAF3 and TRAF6, Nature 439 (2006) 204–207.
[39] A. Heim, M. Stille-Siegener, R. Kandolf, H. Kreuzer, H.R. Figulla, Enterovirus-induced myocarditis: hemodynamic deterioration with immunosuppressive therapy and successful application of interferon-alpha, Clin. Cardiol. 17 (1994) 563–565.
[40] G.H. Holm, A.J. Pruijssers, L. Li, P. Danthi, B. Sherry, T.S. Dermody, Interferon regulatory factor 3 attenuates reovirus myocarditis and contributes to viral clearance, J. Virol. 84 (2010) 6900–6908.
[41] G.H. Holm, J. Zurney, V. Tumilasci, S. Leveille, P. Danthi, J. Hiscott, B. Sherry, T.S. Dermody, Retinoic acid-inducible gene-I and interferon-beta promoter stimulator-1 augment proapoptotic responses following mammalian reovirus infection via interferon regulatory factor-3, J. Biol. Chem. 282 (2007) 21953–21961.
[42] S.M. Horner, H.M. Liu, H.S. Park, J. Briley, M. Gale Jr., Mitochondrial-associated endoplasmic reticulum membranes (MAM) form innate immune synapses and are targeted by hepatitis C virus, Proc. Natl. Acad. Sci. U. S. A. 108 (2011) 14590–14595.
[43] S.M. Horner, C. Wilkins, S. Badil, J. Iskarpatyoti, M. Gale Jr., Proteomic analysis of mitochondrial-associated ER membranes (MAM) during RNA virus infection reveals dynamic changes in protein and organelle trafficking, PLoS One 10 (2015) e0117963.
[44] F. Hou, L. Sun, H. Zheng, B. Skaug, Q.X. Jiang, Z.J. Chen, MAVS forms functional prion-like aggregates to activate and propagate antiviral innate immune response, Cell 146 (2011) 448–461.
[45] S.C. Irvin, J. Zurney, L.S. Ooms, J.D. Chappell, T.S. Dermody, B. Sherry, A single-amino-acid polymorphism in reovirus protein mu2 determines repression of interferon signaling and modulates myocarditis, J. Virol. 86 (2012) 2302–2311.
[46] N. Ishihara, Y. Eura, K. Mihara, Mitofusin 1 and 2 play distinct roles in mitochondrial fusion reactions via GTPase activity, J. Cell Sci. 117 (2004) 6535–6546.
[47] H. Ishikawa, G.N. Barber, STING is an endoplasmic reticulum adaptor that facilitates innate immune signalling, Nature 455 (2008) 674–678.
[48] D.C. Kang, R.V. Gopalkrishnan, Q. Wu, E. Jankowsky, A.M. Pyle, P.B. Fisher, mda-5: an interferon-inducible putative RNA helicase with double-stranded RNA-dependent ATPase activity and melanoma growth-suppressive properties, Proc. Natl. Acad. Sci. U. S. A. 99 (2002) 637–642.
[49] H. Kato, O. Takeuchi, S. Sato, M. Yoneyama, M. Yamamoto, K. Matsui, S. Uematsu, A. Jung, T. Kawai, K.J. Ishii, O. Yamaguchi, K. Otsu, T. Tsujimura, C.S. Koh, C. Reis e Sousa, Y. Matsuura, T. Fujita, S. Akira, Differential roles of MDA5 and RIG-I helicases in the recognition of RNA viruses, Nature 441 (2006) 101–105.
[50] S.J. Kim, M. Khan, J. Quan, A. Till, S. Subramani, A. Siddiqui, Hepatitis B virus disrupts mitochondrial dynamics: induces fission and mitophagy to attenuate apoptosis, PLoS Pathog. 9 (2013) e1003722.
[51] N. Kishore, Q.K. Huynh, S. Mathialagan, T. Hall, S. Rouw, D. Creely, G. Lange, J. Caroll, B. Reitz, A. Donnelly, H. Boddupalli, R.G. Combs, K. Kretzmer, C.S. Tripp, IKK-i and TBK-1 are enzymatically distinct from the homologous enzyme IKK-2: comparative analysis of recombinant human IKK-i, TBK-1, and IKK-2, J. Biol. Chem. 277 (2002) 13840–13847.
[52] T. Koshiba, K. Yasukawa, Y. Yanagi, S. Kawabata, Mitochondrial membrane potential is required for MAVS-mediated antiviral signaling, Sci. Signal. 4 (2011) ra7.
[53] J.D. Lajiness, S.J. Conway, Origin, development, and differentiation of cardiac fibroblasts, J. Mol. Cell. Cardiol. 70 (2014) 2–8.
[54] L. Li, B. Sherry, IFN-alpha expression and antiviral effects are subtype and cell type specific in the cardiac response to viral infection, Virology 396 (2010) 59–68.
[55] H.M. Liu, Y.M. Loo, S.M. Horner, G.A. Zornetzer, M.G. Katze, M. Gale Jr., The mitochondrial targeting chaperone 14-3-3epsilon regulates a RIG-I translocon that mediates membrane association and innate antiviral immunity, Cell Host Microbe 11 (2012) 528–537.
[56] S. Liu, J. Chen, X. Cai, J. Wu, X. Chen, Y.T. Wu, L. Sun, Z.J. Chen, MAVS recruits multiple ubiquitin E3 ligases to activate antiviral signaling cascades, elife 2 (2013) e00785.
[57] T. Maniatis, J.V. Falvo, T.H. Kim, T.K. Kim, C.H. Lin, B.S. Parekh, M.G. Wathelet, Structure and function of the interferon-beta enhanceosome, Cold Spring Harb. Symp. Quant. Biol. 63 (1998) 609–620.
[58] I. Marie, J.E. Durbin, D.E. Levy, Differential viral induction of distinct interferon-alpha genes by positive feedback through interferon regulatory factor-7, EMBO J. 17 (1998) 6660–6669.
[59] I. Marie, E. Smith, A. Prakash, D.E. Levy, Phosphorylation-induced dimerization of interferon regulatory factor 7 unmasks DNA binding and a bipartite transactivation domain, Mol. Cell. Biol. 20 (2000) 8803–8814.
[60] J. Marin-Garcia, A.T. Akhmedov, Mitochondrial dynamics and cell death in heart failure, Heart Fail. Rev. 21 (2016) 123–136.
[61] E. Meylan, J. Curran, K. Hofmann, D. Moradpour, M. Binder, R. Bartenschlager, J. Tschopp, Cardif is an adaptor protein in the RIG-I antiviral pathway and is targeted by hepatitis C virus, Nature 437 (2005) 1167–1172.
[62] M. Miric, A. Miskovic, J.D. Vasiljevic, N. Keserovic, M. Pesic, Interferon and thymic hormones in the therapy of human myocarditis and idiopathic dilated cardiomyopathy, Eur. Heart J. 16 (Suppl. 0) (1995) 150–152.
[63] D. Naon, M. Zaninello, M. Giacomello, T. Varanita, F. Grespi, S. Lakshminaranayan, A. Serafini, M. Semenzato, S. Herkenne, M.I. Hernández-Alvarez, A. Zorzano, D. De Stefani, G.W. Dorn, L. Scorrano, Critical reappraisal confirms that Mitofusin 2 is an endoplasmic reticulum–mitochondria tether, Proc. Natl. Acad. Sci. 113 (2016) 11249–11254.
[64] D.L. Noah, M.A. Blum, B. Sherry, Interferon regulatory factor 3 is required for viral induction of beta interferon in primary cardiac myocyte cultures, J. Virol. 73 (1999) 10208–10213.
[65] G. Oganesyan, S.K. Saha, B. Guo, J.Q. He, A. Shahangian, B. Zarnegar, A. Perry, G. Cheng, Critical role of TRAF3 in the Toll-like receptor-dependent and -independent antiviral response, Nature 439 (2006) 208–211.
[66] K. Onoguchi, K. Onomoto, S. Takamatsu, M. Jogi, A. Takemura, S. Morimoto, I. Julkunen, H. Namiki, M. Yoneyama, T. Fujita, Virus-infection or 5'ppp-RNA activates antiviral signal through redistribution of IPS-1 mediated by MFN1, PLoS Pathog. 6 (2010) e1001012.
[67] K.N. Papanicolaou, R.J. Khairallah, G.A. Ngoh, A. Chikando, I. Luptak, K.M. O'Shea, D.D. Riley, J.J. Lugus, W.S. Colucci, W.J. Lederer, W.C. Stanley, K. Walsh, Mitofusin-2 maintains mitochondrial structure and contributes to stress-induced permeability transition in cardiac myocytes, Mol. Cell. Biol. 31 (2011) 1309–1328.
[68] K.N. Papanicolaou, R. Kikuchi, G.A. Ngoh, K.A. Coughlan, I. Dominguez, W.C. Stanley, K. Walsh, Mitofusins 1 and 2 are essential for postnatal metabolic remodeling in heart, Circ. Res. 111 (2012) 1012–1026.
[69] S. Paz, M. Vilasco, S.J. Werden, M. Arguello, D. Joseph-Pillai, T. Zhao, T.L. Nguyen, Q. Sun, E.F. Meurs, R. Lin, J. Hiscott, A functional C-terminal TRAF3-binding site in MAVS participates in positive and negative regulation of the IFN antiviral response, Cell Res. 21 (2011) 895–910.
[70] E.E. Rivera-Serrano, B. Sherry, NF-kappaB activation is cell type-specific in the heart, Virology 502 (2017) 133–143.
[71] D.M. Rothwarf, E. Zandi, G. Natoli, M. Karin, IKK-gamma is an essential regulatory subunit of the IkappaB kinase complex, Nature 395 (1998) 297–300.

[72] M. Sato, N. Hata, M. Asagiri, T. Nakaya, T. Taniguchi, N. Tanaka, Positive feedback regulation of type I IFN genes by the IFN-inducible transcription factor IRF-7, FEBS Lett. 441 (1998) 106–110.
[73] S. Schmid, D. Sachs, B.R. tenOever, Mitogen-activated protein kinase-mediated licensing of interferon regulatory factor 3/7 reinforces the cell response to virus, J. Biol. Chem. 289 (2014) 299–311.
[74] C.A. Schneider, W.S. Rasband, K.W. Eliceiri, NIH image to ImageJ: 25 years of image analysis, Nat. Methods 9 (2012) 671–675.
[75] J.W. Schoggins, C.M. Rice, Interferon-stimulated genes and their antiviral effector functions, Curr. Opin. Virol. 1 (2011) 519–525.
[76] H.P. Schultheiss, C. Piper, O. Sowade, F. Waagstein, J.F. Kapp, K. Wegscheider, G. Groetzbach, M. Pauschinger, F. Escher, E. Arbustini, H. Siedentop, U. Kuehl, Betaferon in chronic viral cardiomyopathy (BICC) trial: effects of interferon-beta treatment in patients with chronic viral cardiomyopathy, Clin. Res. Cardiol. 105 (2016) 763–773.
[77] K.L. Schultz, P.S. Vernon, D.E. Griffin, Differentiation of neurons restricts Arbovirus replication and increases expression of the alpha isoform of IRF-7, J. Virol. 89 (2015) 48–60.
[78] R.B. Seth, L. Sun, C.K. Ea, Z.J. Chen, Identification and characterization of MAVS, a mitochondrial antiviral signaling protein that activates NF-kappaB and IRF 3, Cell 122 (2005) 669–682.
[79] S. Sharma, B.R. tenOever, N. Grandvaux, G.P. Zhou, R. Lin, J. Hiscott, Triggering the interferon antiviral response through an IKK-related pathway, Science (New York, N.Y.) 300 (2003) 1148–1151.
[80] B. Sherry, Generating primary cultures of murine cardiac myocytes and cardiac fibroblasts to study viral myocarditis, Methods Mol. Biol. 1299 (2015) 1–16.
[81] B. Sherry, C.J. Baty, M.A. Blum, Reovirus-induced acute myocarditis in mice correlates with viral RNA synthesis rather than generation of infectious virus in cardiac myocytes, J. Virol. 70 (1996) 6709–6715.
[82] B. Sherry, B.N. Fields, The reovirus M1 gene, encoding a viral core protein, is associated with the myocarditic phenotype of a reovirus variant, J. Virol. 63 (1989) 4850–4856.
[83] B. Sherry, X.Y. Li, K.L. Tyler, J.M. Cullen, H.W.T. Virgin, Lymphocytes protect against and are not required for reovirus-induced myocarditis, J. Virol. 67 (1993) 6119–6124.
[84] B. Sherry, F.J. Schoen, E. Wenske, B.N. Fields, Derivation and characterization of an efficiently myocarditic reovirus variant, J. Virol. 63 (1989) 4840–4849.
[85] B. Sherry, J. Torres, M.A. Blum, Reovirus induction of and sensitivity to beta interferon in cardiac myocyte cultures correlate with induction of myocarditis and are determined by viral core proteins, J. Virol. 72 (1998) 1314–1323.
[86] M.H. Soonpaa, M. Rubart, L.J. Field, Challenges measuring cardiomyocyte renewal, Biochim. Biophys. Acta 1833 (2013) 799–803.
[87] M.J. Stewart, K. Smoak, M.A. Blum, B. Sherry, Basal and reovirus-induced beta interferon (IFN-beta) and IFN-beta-stimulated gene expression are cell type specific in the cardiac protective response, J. Virol. 79 (2005) 2979–2987.
[88] M.S. Suthar, H.J. Ramos, M.M. Brassil, J. Netland, C.P. Chappell, G. Blahnik, A. McMillan, M.S. Diamond, E.A. Clark, M.J. Bevan, M. Gale Jr., The RIG-I-like receptor LGP2 controls CD8(+) T cell survival and fitness, Immunity 37 (2012) 235–248.
[89] E.D. Tang, C.Y. Wang, MAVS self-association mediates antiviral innate immune signaling, J. Virol. 83 (2009) 3420–3428.
[90] J.G. Travers, F.A. Kamal, J. Robbins, K.E. Yutzey, B.C. Blaxall, Cardiac fibrosis: the fibroblast awakens, Circ. Res. 118 (2016) 1021–1040.
[91] P.H. Tseng, A. Matsuzawa, W. Zhang, T. Mino, D.A. Vignali, M. Karin, Different modes of ubiquitination of the adaptor TRAF3 selectively activate the expression of type I interferons and proinflammatory cytokines, Nat. Immunol. 11 (2010) 70–75.
[92] J.H. van Berlo, J.D. Molkentin, An emerging consensus on cardiac regeneration, Nat. Med. 20 (2014) 1386–1393.
[93] W.J. van Zuylen, P. Doyon, J.F. Clement, K.A. Khan, L.M. D'Ambrosio, F. Do, M. St-Amant-Verret, T. Wissanji, G. Emery, A.C. Gingras, S. Meloche, M.J. Servant, Proteomic profiling of the TRAF3 interactome network reveals a new role for the ER-to-Golgi transport compartments in innate immunity, PLoS Pathog. 8 (2012) e1002747.
[94] C. Vazquez, S.M. Horner, MAVS coordination of antiviral innate immunity, J. Virol. 89 (2015) 6974–6977.
[95] H.W. Virgin, M.A. Mann, B.N. Fields, K.L. Tyler, Monoclonal antibodies to reovirus reveal structure/function relationships between capsid proteins and genetics of susceptibility to antibody action, J. Virol. 65 (1991) 6772–6781.
[96] J. Wang, L.H. Aung, B.S. Prabhakar, P. Li, The mitochondrial ubiquitin ligase plays an anti-apoptotic role in cardiomyocytes by regulating mitochondrial fission, J. Cell. Mol. Med. 20 (2016) 2278–2288.
[97] M.G. Wathelet, C.H. Lin, B.S. Parekh, L.V. Ronco, P.M. Howley, T. Maniatis, Virus infection induces the assembly of coordinately activated transcription factors on the IFN-beta enhancer in vivo, Mol. Cell 1 (1998) 507–518.
[98] I. Weibrecht, K.J. Leuchowius, C.M. Clausson, T. Conze, M. Jarvius, W.M. Howell, M. Kamali-Moghaddam, O. Soderberg, Proximity ligation assays: a recent addition to the proteomics toolbox, Expert. Rev. Proteomics 7 (2010) 401–409.
[99] A.P. West, G.S. Shadel, S. Ghosh, Mitochondria in innate immune responses, Nat. Rev. Immunol. 11 (2011) 389–402.
[100] D.R. Wilcox, S.S. Folmsbee, W.J. Muller, R. Longnecker, the type I interferon response determines differences in choroid plexus susceptibility between newborns and adults in herpes simplex virus encephalitis, mBio (2016) 7.
[101] B. Wu, S. Hur, How RIG-I like receptors activate MAVS, Curr. Opin. Virol. 12 (2015) 91–98.
[102] L.G. Xu, Y.Y. Wang, K.J. Han, L.Y. Li, Z. Zhai, H.B. Shu, VISA is an adapter protein required for virus-triggered IFN-beta signaling, Mol. Cell 19 (2005) 727–740.
[103] S. Yamaoka, G. Courtois, C. Bessia, S.T. Whiteside, R. Weil, F. Agou, H.E. Kirk, R.J. Kay, A. Israel, Complementation cloning of NEMO, a component of the IkappaB kinase complex essential for NF-kappaB activation, Cell 93 (1998) 1231–1240.
[104] K. Yasukawa, H. Oshiumi, M. Takeda, N. Ishihara, Y. Yanagi, T. Seya, S. Kawabata, T. Koshiba, Mitofusin 2 inhibits mitochondrial antiviral signaling, Science Signal. 2 (2009) ra47.
[105] M. Yoneyama, M. Kikuchi, T. Natsukawa, N. Shinobu, T. Imaizumi, M. Miyagishi, K. Taira, S. Akira, T. Fujita, The RNA helicase RIG-I has an essential function in double-stranded RNA-induced innate antiviral responses, Nat. Immunol. 5 (2004) 730–737.
[106] C.Y. Yu, J.J. Liang, J.K. Li, Y.L. Lee, B.L. Chang, C.I. Su, W.J. Huang, M.M. Lai, Y.L. Lin, Dengue virus impairs mitochondrial fusion by cleaving mitofusins, PLoS Pathog. 11 (2015) e1005350.
[107] E. Zandi, D.M. Rothwarf, M. Delhase, M. Hayakawa, M. Karin, The IkappaB kinase complex (IKK) contains two kinase subunits, IKKalpha and IKKbeta, necessary for IkappaB phosphorylation and NF-kappaB activation, Cell 91 (1997) 243–252.
[108] M.M. Zaruba, L.J. Field, The mouse as a model system to study cardiac regeneration, Drug Discov. Today Dis. Model. 5 (2008) 165–171.
[109] S. Zhang, X. Bu, H. Zhao, J. Yu, Y. Wang, D. Li, C. Zhu, T. Zhu, T. Ren, X. Liu, L. Yao, J. Su, A host deficiency of discoidin domain receptor 2 (DDR2) inhibits both tumour angiogenesis and metastasis, J. Pathol. 232 (2014) 436–448.
[110] R. Zhou, A.S. Yazdi, P. Menu, J. Tschopp, A role for mitochondria in NLRP3 inflammasome activation, Nature 469 (2011) 221–225.
[111] J. Zurney, K.E. Howard, B. Sherry, Basal expression levels of IFNAR and Jak-STAT components are determinants of cell-type-specific differences in cardiac antiviral responses, J. Virol. 81 (2007) 13668–13680.
[112] J. Zurney, T. Kobayashi, G.H. Holm, T.S. Dermody, B. Sherry, Reovirus mu2 protein inhibits interferon signaling through a novel mechanism involving nuclear accumulation of interferon regulatory factor 9, J. Virol. 83 (2009) 2178–2187.